



PILOT STUDY OF ICE-STRUCTURE INTERACTION IN A PENDULUM ACCELERATOR

Martin Storheim^{1,2,3}, Torodd Nord², Ekaterina Kim^{1,2,3}, Knut Høyland², Magnus Langseth⁴,
Jørgen Amdahl^{1,2,3}, Sveinung Løset²

¹ Department of Marine Technology, Norwegian University of Science and Technology, Trondheim,
Norway

² Centre for Sustainable Arctic Marine and Coastal Technology (SAMCoT), Norwegian University of
Science and Technology, Trondheim, Norway

³ Centre for Autonomous Marine Operations and Systems (AMOS), Center of Excellence, Norwegian
University of Science and Technology, Trondheim, Norway

⁴ Structural Impact Laboratory (SIMLab) – Centre for Research-based Innovation, Norwegian
University of Science and Technology, Trondheim, Norway

ABSTRACT

More knowledge on the coupled response of ice and structure in collision in which both bodies undergo permanent damage is needed. These types of experiments are challenging to perform in a laboratory at relatively high impact speeds. A pendulum accelerator impact rig was used to overcome the aforementioned challenge, in which an ice mass was attached to a trolley and accelerated into a structure at a speed of 8 m/s. Four freshwater granular ice samples were impacted onto flexible steel beams. The impacts resulted in crushing of the ice samples while recoverable and unrecoverable deformations were observed in the beams. Force and displacement histories were recorded along with high-speed video of the ice and steel structure deformations. This paper describes the test setup, instrumentation and ice manufacturing, and presents the main test results.

INTRODUCTION

The design loads used when designing low ice-class vessels (e.g. Baltic ice class 1A+) are low, and the vessels are expecting damage during their service life, see Riska and Kämäräinen (2011). If this damage is small, repairs can be performed on the next classification of the vessel, whereas larger damages should get immediate attention. As discussed by Kujala and Ehlers (2013), the choice of a design load level that causes no damage will then be a matter of cost optimization.

This method gives cost effective ships. The direct alternative is to calculate the load with a 100-year return period, similar to what is done for normal ships and offshore structures. This would significantly increase the vessel scantlings, and thereby increase the investment cost and decrease the cargo capacity for a fixed vessel size.

An additional requirement against extreme damage should be placed on the vessel designs which have a design load with annual probability less than e.g. 100 years, to ensure that the damage from an event outside of the design limits does give catastrophic consequences. This is especially relevant for vessels e.g. in the Northern Sea Route, for which low ice-class vessels are allowed provided light ice conditions and icebreaker assistance. Several scenarios with loading above the design point are to be expected, e.g. by travelling with a too high speed compared to the plausible impact loads from multi-year ice floes or bergy bits.

As these extreme load scenarios could involve severe damage to both the ice and vessel, the coupled behaviour of ice and structure during deformation is important. The impact force will now depend on the evolution of structural deformations, and force redistribution can occur during the impact. Additionally, the coupled response may lead to an increase in the

confinement (change of local stress state) of the ice, thereby increasing its crushing strength. A recent example of potentially critical damage from ice collisions is the oil tanker *Nordvik*, which collided with an ice mass in 2013 causing water ingress (Pettersen 2013). The vessel had a low ice class, but was still permitted to sail in Arctic conditions during the summer season.

Most typical full-scale impact scenarios that can lead to structural damage will occur at high indentation velocities, either caused by the vessel speed or wave-induced motions of the ice, while other common damages result from compression forces in an ice sheet at near quasi-static conditions (Hänninen 2005). Realistic impacts are thus in the brittle ice regime (Schulson and Duval 2009), and is the focus of this paper.

The literature contains only a few experiments with coupled interaction between ice and structure and permanent damage to both interacting bodies. Full-scale ice impacts were conducted with the icebreaker *Kigoriak* (Varsta and Riska 1982), in which a few cases exceeded the elastic load limit. In the field test campaign at the Hobson's Choice ice island, flat indenters were pushed against an ice wedge at constant speeds, see Masterson et al. (1993). Quasi-static experiments have been performed in the STePS² program (see Manuel et al. 2013), where the ice failure was in a ductile-dominated regime, far from what normally is experienced in full-scale impacts. Further, high strain-rate behaviour of ice has been investigated by several researchers, e.g. field drop-rig experiments on rigid pipes (Saeki et al. 1977), pendulum impact experiments on spherical indenter into confined ice (Oldford et al. 2014) or using a split Hopkinson pressure bar in Shazly et al. (2008), but none of these are coupled to the inelastic structural response.

There is a need for deeper understanding of the brittle ice behaviour during impacts in which both the ice and structure undergo large inelastic deformations, and where contact surfaces do not remain flat. The present paper describes a pilot study of laboratory impact experiments that could help to mitigate this knowledge gap.

EXPERIMENTAL SETUP

The experiments were conducted in the *pendulum accelerator* impact rig at the SIMLab laboratory facilities at NTNU, Trondheim. The pendulum accelerator uses a pendulum arm to accelerate a trolley along a set of rails towards an impacted structure. The impacted structure is attached to a 150 ton concrete reaction wall on rubber foundations to resist the impact. The impact rig can be used with varying trolley mass and impact speeds. The pendulum impact rig is thoroughly described in Hanssen et al. (2003).

In these experiments, the trolley mass was 711.5 kg and the impact velocity 8 m/s. An ice piece was attached to the front of the trolley through a steel adapter (Figure 1), which also provided boundary conditions for the aft end of the ice. The kinetic energies for the experiments were in the range of 24 kJ. If all kinetic energy was not absorbed by the ice impact, a secondary barrier system stopped the trolley and prevented damage to the impact rig and measurement equipment.

No scale was defined as such for the experiments; the focus was rather to obtain results from impacts between freshwater granular ice and steel in a realistic impact scenario causing structural damage and a coupled ice-structure response.

Ice sample preparation

Glacial ice, and to some extent multi-year ice, have a predominant granular structure and low or no salinity. To get ice behaviour close to this, granular freshwater ice was manufactured using commercially available crushed ice and cooled freshwater. The ice manufacturing was influenced by the recommendations from the STePS²-program reported in Gudimetla et al. (2012) and the lessons learned in the experiments reported in Kim et al. (2013).



Figure 1 Ice sample mounted to the trolley.

Circular ice specimens were preferred to attach the specimen to the impact trolley and to reduce effects of sharp boundaries on the ice response. The steel adapter connecting the ice sample to the trolley (Figure 1) consists of a bolt plate, a cylindrical spacer and a 20 mm thick backing plate, which act as the end support of the ice specimen. Forward of the backing plate, a steel cylinder with internal diameter of 320 mm, a thickness of 4 mm and a height of 100 mm (impacts 1-3) and 200 mm (impact 4) served to hold the cantilevered ice sample in place prior to impact, as well as adding some confinement to the aft end of the ice sample. Six 50 mm bolts were inserted radially in the top of the confining steel cylinder to better anchor the ice to the adapter.

In the ice manufacturing procedure, the steel adapter was resting vertically on the cold room floor. A thin plastic pipe was attached above the steel adapter using water and duct tape to create a mold for the freezing process, giving a maximum sample height of around 500 mm. The mold assembly was left to cool prior to the ice sample manufacturing. Once cooled, the mold was filled with layers of commercially available crushed ice, commonly used for fish storage, mixed with cooled freshwater. The crushed ice had a seed size varying from 2 to 20 mm (Figure 2). The larger pieces were not complete crystals, but rather smaller ice pieces sintered together. The mixture was stirred throughout the filling process to prevent large air entrapments.

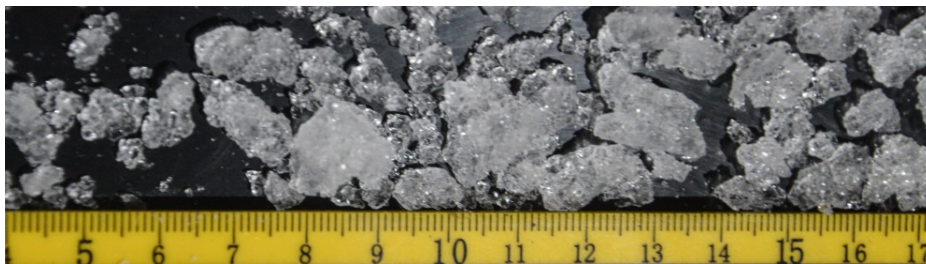


Figure 2 Commercially available crushed ice.

Once the samples were fully mixed, sample 1-3 were insulated on the sides and partly on the top to obtain a near unidirectional freezing from the bottom towards the ice tip, thereby reducing thermal stresses and cracks. Sample 4 was left without insulation. The samples were then left to freeze for three days.

When the samples were completely frozen, the plastic bucket was carefully cut away using an angle grinder. Due to time limitations a proper shaping apparatus was not available, in which a symmetric easily defined shape could be obtained. The ice was shaped using an angle grinder with a wood sander disc of grade 80. The grinding was very suitable for the ice shaping, but the manual control resulted in slightly asymmetric ice shapes.

A bullet-like shape was targeted, with a free cylindrical portion of the ice still intact to limit the confining effect of the steel cylinder on the ice response. The four samples are shown in

Figure 3a. Ice sample 2 had a visible circumferential healed crack at the tip of the sample. The other samples showed no visible cracks. Figure 3b shows the measured shape of the specimens, extracted from images of the ice specimen by a high-speed camera directly above the impact location prior to impact.

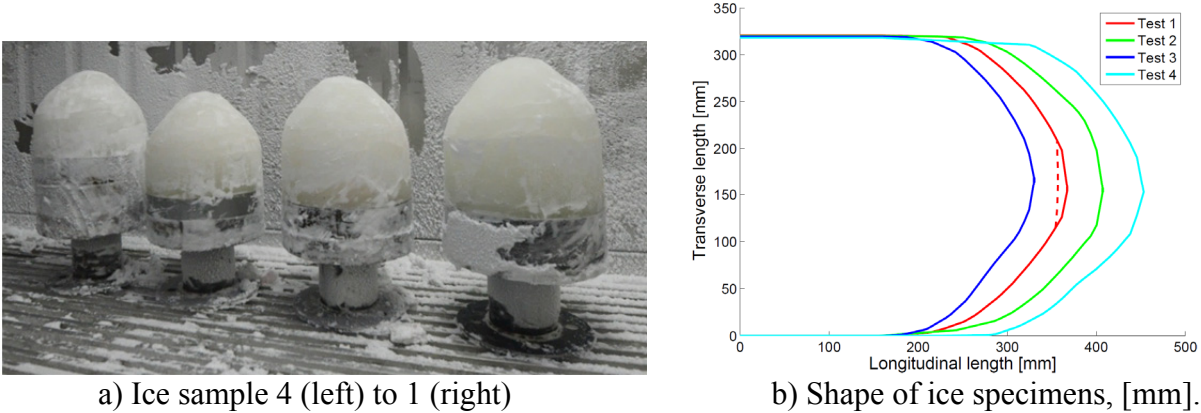


Figure 3 Shape of ice samples after shaping. Dashed line in b) indicate initial circumferential crack in specimen 2 (test 1).

Figure 4 shows a thin-section of the intact ice. The grain size is around 1-5 mm. Small air bubbles were distributed in the ice, remnants of the original crushed ice structure. The ice microstructure has many similarities to iceberg ice, but the shape of the grains and their interlocking as well as the character of air bubble accumulation differs, see Gagnon and Gammon (1995) and Barrette and Jordaan (2001) for details of iceberg ice properties. The ice was stored for two days after shaping at -24°C.

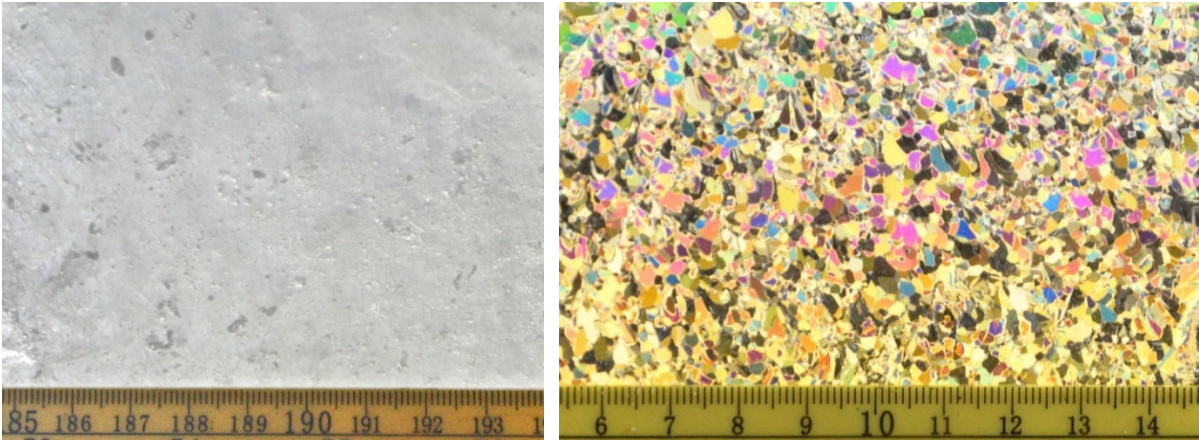


Figure 4 Air inclusions and a thin-section of ice as produced. Ruler scale in [cm].

Impacted structure

The target of the experiment was to achieve a coupled ice-structure interaction. Thus, the steel should be strong enough to crush the ice, but weak enough to also dissipate plastic energy itself. The width of rail system in the impact rig prevented the use of a plate structure as the struck object. Instead, a hollow profile beam with dimensions 140×80×6 mm was selected, wide enough to cover most of the expected contact area of the collision. The beam was mounted on simple supports in which the span length could be varied (Figure 5).

The steel grade was S355J2H. Four uniaxial tensile samples, two from each side of the beam, were tested at a speed of 2.1 mm/min. The cross-section varied from 5.83-5.94 by 12.43-12.57 mm. Two extensometers with gauge length 35 mm, one on either side of the specimen, measured the displacements accurately up to 4.5 mm elongation (13% strain). In addition, the

stroke of the uniaxial test apparatus was measured (includes the complete specimen and elastic response of the clamping system). The latter was used to estimate the response after 13% strain, calibrated to match the extensometer response. Figure 6 shows the test results in engineering stress vs. strain. The material response was found to be well represented by a Young's modulus $E=194$ GPa, a yield stress of 460 MPa, and power law modulus $K=798$ MPa and exponent $n=0.157$. No strain-rate tests were performed, but this is recommended for a more elaborate impact study.

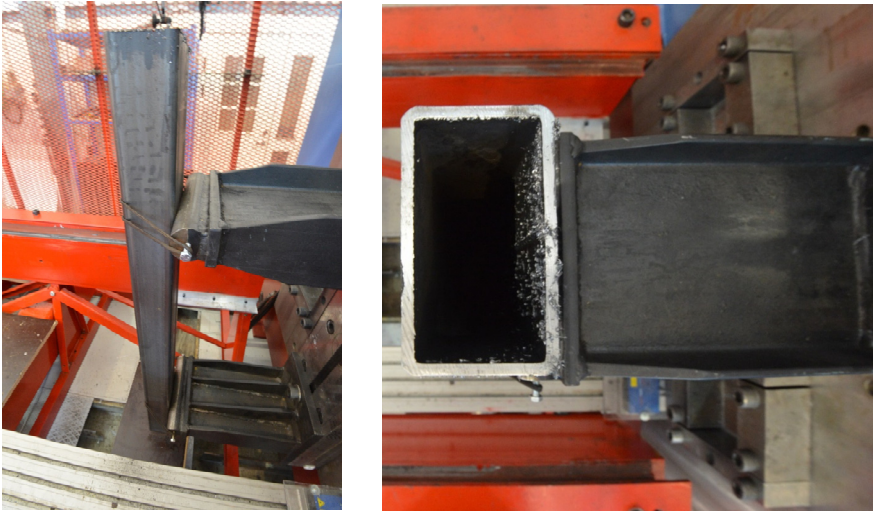


Figure 5 Hollow profile beam mounted on two simple supports. Rubber bands attach the beam to the supports.

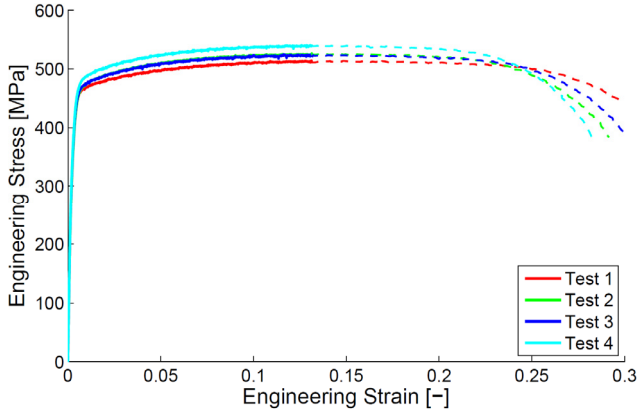


Figure 6 Engineering stress-strain from four uniaxial tensile tests. Solid lines are measured with the extensometers, dashed lines from the stroke of the testing machine (less accurate).

The steel beam was designed weak enough to be able to deform plastically, but strong enough to also crush the ice. This resulted in a natural period of vibration of the beam in the same order of magnitude as the impact event, with the first global natural period of the simply supported beam of around 2 ms.

Measurements

The impact force was measured by a load cell between the trolley and the ice adapter. The load cell was calibrated statically up to 500 kN, though its capacity was far greater. The position of the carriage was measured by a laser distance meter mounted on the rail system. In

addition, a laser measured the deflection of the reaction wall. The wall deflection was found to be negligible during the impacts. The force and distances were recorded at 100 kHz, but the laser measuring the position of the trolley only supplied new data every 2.5 kHz, thereby creating a stepped load signal.

Two Phantom v1610 high-speed cameras recorded the impacts, one from above and one from approximately 45° to the side. The cameras recorded at 18 kHz with a resolution of 1280×720 pixels. The measured force and distance signals were also supplied to the camera system to synchronize the measurements and video recordings.

A laser trigger was activated by the trolley to start the measurements at a fixed distance prior to impact. This triggered both the force and distance measurements as well as the high-speed cameras.

Test matrix

Four impacts were performed using the four ice samples. All impacts had the same trolley mass and the same impact velocity, but the span of the beam and the ice mass were varied. The temperature in the lab was approximately +20°C. In order to minimize the time the ice specimens were exposed to the warm air, they were shielded by a double layer of bubble wrap plastic. This insulation was removed some minutes prior to impact. The ice temperature was around -24°C. The mass, kinetic energy, beam span and time exposed to the +20°C in the lab (warm exposure) are given in Table 1.

Table 1 Test matrix with key parameters.

Test #	Ice sample	Mass of ice and adapter [kg]			Kinetic energy [kJ]	Beam span [mm]	Warm exposure [min]
		before	after	crushed			
1	2	47.7	33.2	-14.5	24.3	700	16
2	1	49.2	33.0	-16.2	24.3	900	10
3	3	45.8	33.5	-12.3	24.2	800	15
4	4	54.4	42.0	-12.4	24.5	800	9

MAIN RESULTS

The measured force-time histories are shown in Figure 7a for all four tests and for the entire impact duration. An initial large load peak (first 10 ms) was observed, at the end of which the ice sample was fractured into individual fragments and contact was partially lost (marked with dashed line in Figure 7a). Some of the tests then obtained a secondary impact, when remaining intact ice regained contact. Large oscillations were observed for all the tests with a period of around 1 ms.

Test 1 showed a significantly larger force peak than the other tests. Figure 7b shows the corresponding force-displacement curve for the first 10 ms of impact. Displacement is here the change in position of the trolley from first contact. Points of interest are marked with letters, and the corresponding deformation of the ice and beam are shown in Figure 8.

The high contact force in test 1 was partially due to a circumferential initial crack on the tip of the specimen (Figure 3b and Figure 8a), that crushed early in the interaction (first 10 mm in Figure 7b). After this, the contact area between the ice and steel was larger, and the ice could withstand a larger force prior to global comminuted fracture of the specimen (starts after point c). At point d in Figure 7b, the ice strength degraded due to accumulation of cracks, and the load level dropped while more and more of the ice lost its integrity and contact. The remaining ice pieces started to move outwards, while some ice blocks still maintained contact between the steel adapter and the steel beam. After point e, no solid ice pieces remained in contact, and the force level dropped significantly while the remaining ice was cleared away.

All four tests showed the same large oscillations with a period of around 1 ms. These are very different from the saw tooth-pattern typically observed in ice crushing events. During the first two large load peaks (from b to c in Figure 7b) no visible damage was observed in the bulk ice other than pulverization at the tip of the sample and small cracks radiating away from the contact zone. At the second large peak (point c), global fractures from the tip to the bottom of the specimens was observed for all tests. The main difference between test 1 and tests 2-4 was the circumferential initial crack, which crushed without causing visible damage to the rest of the ice (a to b in Figure 7b), thereby creating a larger contact area capable of higher force before the sample failed globally.

The oscillations are probably due to interaction with the deflection modes of the impacted beam, both globally as beam vibrations and locally as vibrations of the beam flange. However, the measurement setup of the beam response was not sufficient to substantiate this.

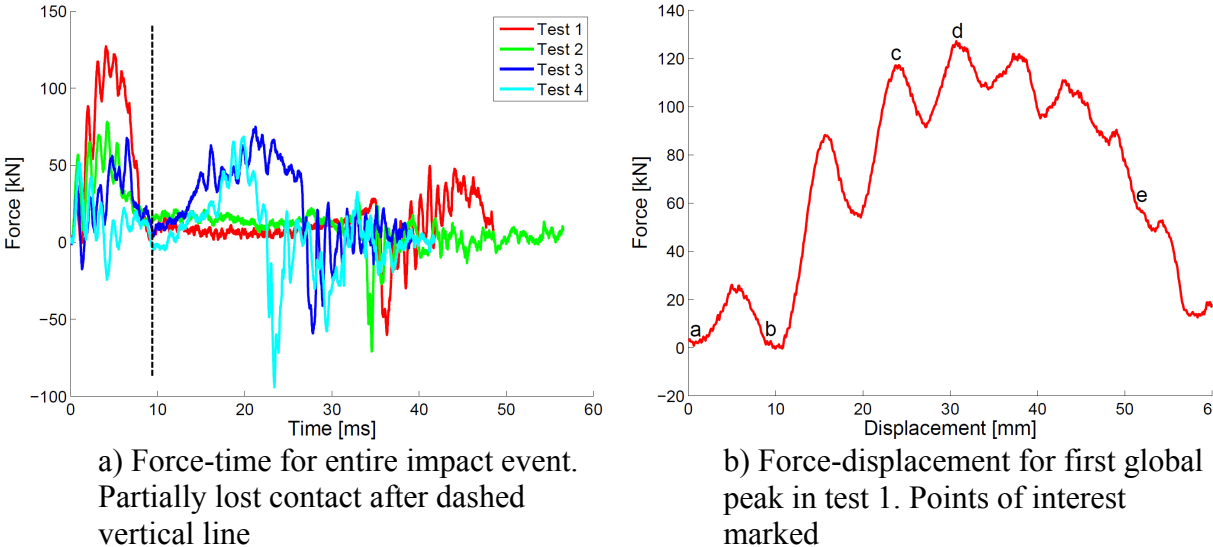


Figure 7 Force-time histories of all tests (left) and force vs. trolley displacement (right) for the first large load peak.

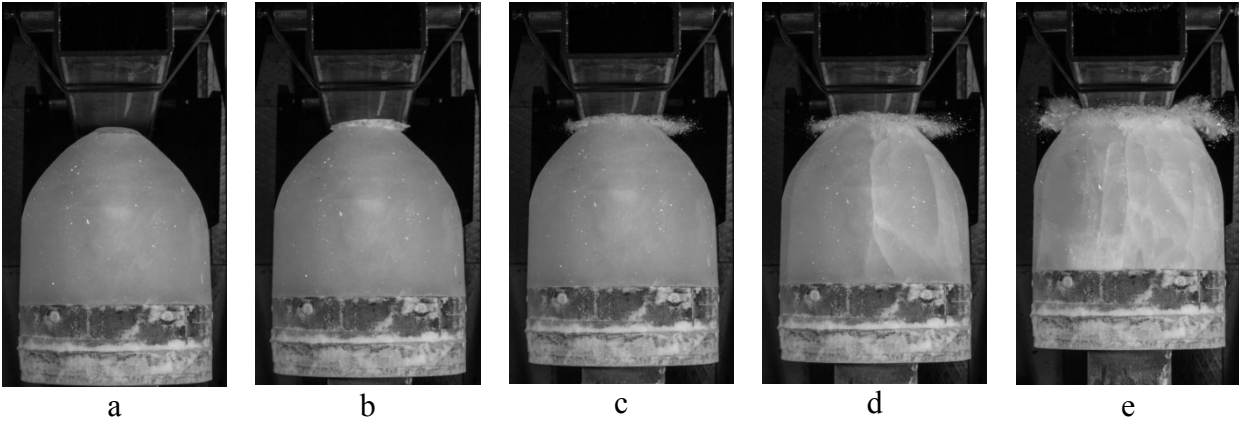


Figure 8 Deformation pattern at marked points in Figure 7b for impact 1.

Figure 9 shows the plastically deformed configuration of the steel beam, measured after impact 1. A global deflection with amplitude of around 10 mm was combined with a local deflection of the beam flange around the impact with an additional 14 mm indentation. The total global deflection during the impact (elastic+plastic) was about 60% larger, and occurred

after approximately 45 mm displacement of the trolley in Figure 7b, somewhat out of phase from the force signal.

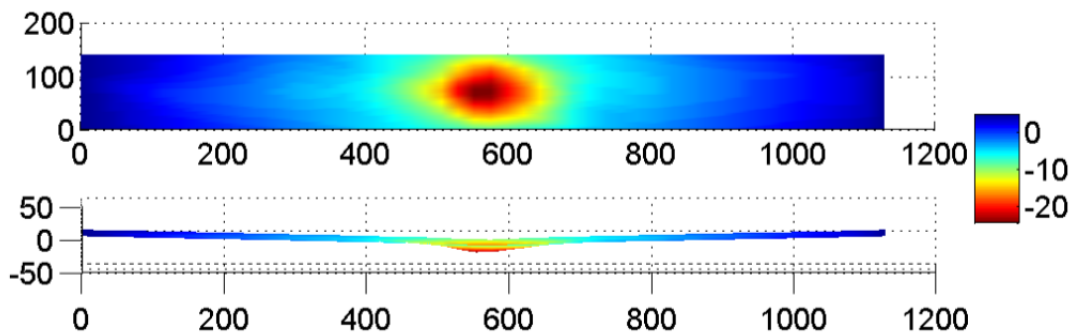


Figure 9 Deformation of steel beam from impact 1. Values in [mm].

The deflection of the beam should be combined with the displacement of the trolley to obtain an estimate of the crushing distance of the ice. The global beam deflection was extracted through processing of the high-speed video files, and an updated force-displacement curve is shown in Figure 10. The corrected curve now represents a better estimate of the actual indentation into the ice, but the local deflection of the beam flange has not been accounted for. This would additionally reduce the estimate of indentation into the ice.

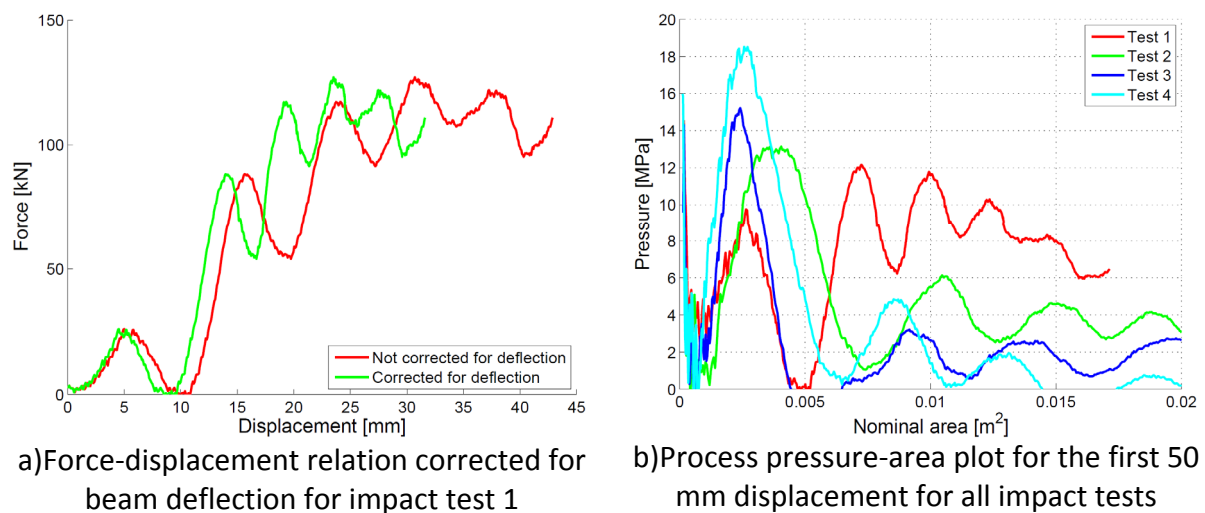


Figure 10 Force-displacement and pressure-area plots. Note that the area for impact 2 -4 is not corrected for the beam deflection.

The crushing distance of the ice is estimated from the displacement of the trolley corrected for global deflection of the beam. Using the shape data in Figure 3b, the nominal contact area is calculated by assuming a circular contact, and used to establish the *process* pressure-area relation in the right of Figure 10 for impact 1. For the other impacts, the elastic deflection of the beam was smaller, and is not accounted for in the area calculation.

For impact test no. 1, crushing of the ice cap gave a high initial pressure. As the larger contact area was established after this, the nominal pressure peaked at 12 MPa. After large fractures were visible in the ice, the rate of increase in pressure vs. area decreased as a result of the accumulated ice damage, both micromechanical and global comminuted fractures. For impacts 2-4, a higher peak pressure was observed at a lower force, after which the pressure capacity of the ice samples decreased quickly. Impact 1 showed a slower decrease in pressure capacity, likely due to the confining effect from the plastically deformed beam.

Comparing the obtained pressure-area data with literature shows that the ice behaviour is in line with other published data of crushing of freshwater ice, see Figure 11. Ulan-Kvitberg et al. (2011) investigated the effect of constrained and unconstrained ice cones (thereby different levels of local confinement of the ice) on ice with a "high degree of variability in grain orientation". The constrained samples had a conical shape extending outside from a confining metal cylinder, and the unconstrained samples a cylindrical extension of ice outwards of the confining cylinder before the conically shaped section. The unconstrained samples thus resemble the ice shapes in this study (Figure 3) which also has a cylindrical extension between the shaped tip and the confining cylinder. The results of the present study in test 1 are in line with the values from the constrained tests, indicating that the level of confinement from the deforming steel beam was sufficient to increase the crushing strength of the ice significantly. For tests 2-4, the steel beam did not provide increased confinement and the decreasing pressure trend vs. area match that of the unconstrained tests by Ulan-Kvitberg et al.

The present experiments give pressures in the same range as other experiments with freshwater granular ice, as the Pond Inlet experiments with a 0.1 m² spherical indenter into an ice wall from Masterson and Frederking (1993). The impacts from the double pendulum swing in Oldford et al. (2014) are in the same pressure range, but for lower areas. Note that the impact velocity varies significantly between the reported experiments, with 100 mm/s in Ulan-Kvitberg et al. and the Pond Inlet tests, 2.3-4.7 m/s in Oldford et al. and 8 m/s in the present study.

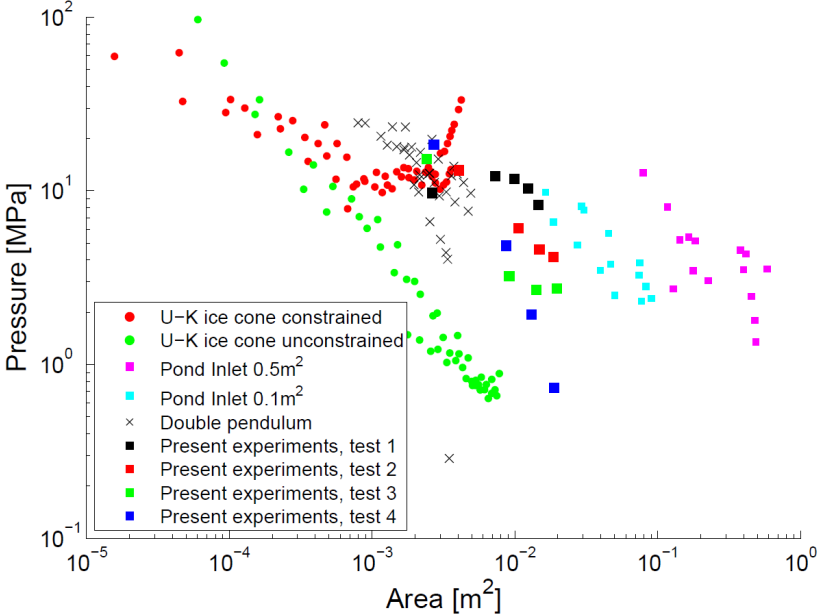


Figure 11 Process pressure-area from impact test 1 compared with data from Pond Inlet-tests (Masterson and Frederking 1993), constrained and unconstrained ice cones (Ulan-Kvitberg et al. 2011) and medium scale impact tests in a double pendulum swing (Oldford et al. 2014). The pressures represent peaks in force-displacement relation, thus giving multiple points pr. experiment

A section of damaged ice was extracted from the contact zone of the secondary force peak in impact 1, and shaved into a thin-section (Figure 12) using a microtome. A compacted crushed layer of ice was present in the top layer, extending about 25 mm into the ice. Inwards of this, the crystal structure is similar to the intact ice in Figure 4.

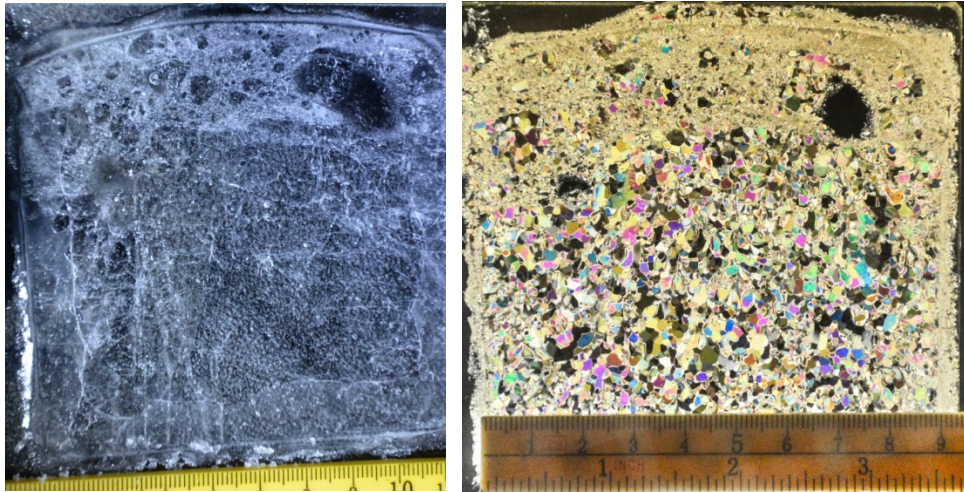


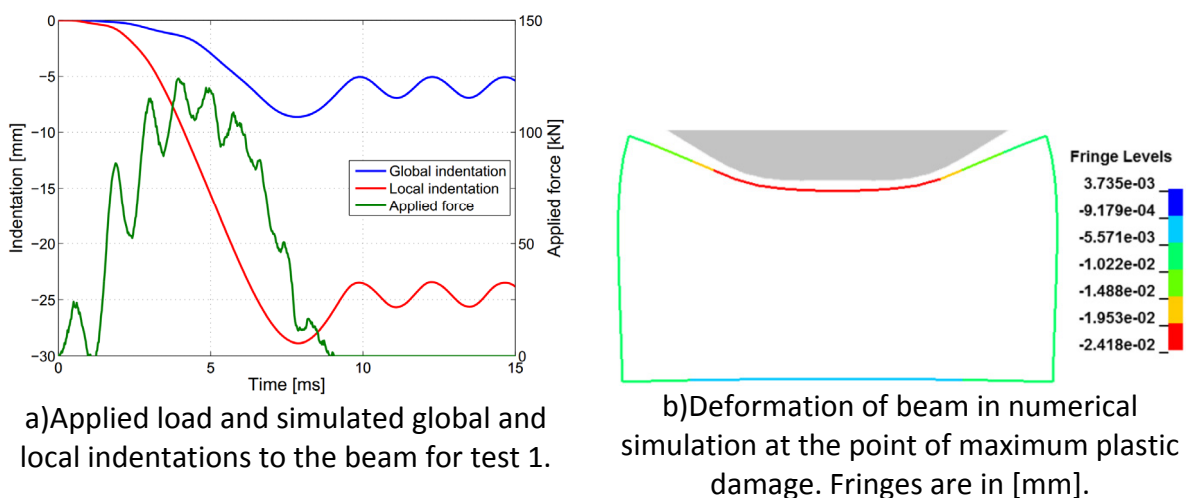
Figure 12 Thin-section of damaged section of ice under side-light (left) and cross-polarized light (right).

CAPACITY EVALUATION OF THE IMPACTED BEAM

The elastic moment capacity of the beam was 160 kN for test 1, i.e. well above the obtained force. Thus, the global deformation was due to local damage to the beam causing contractions on one side of the beam. To better understand the experimental results, the beam response was investigated through finite element analysis. The beam was modelled on simple supports using shell elements with a refined mesh. Power law hardening without strain-rate effects was adopted. The shape of the ice indenter was represented by rigid solid elements based on Figure 3.

The ice indenter was subjected to a transient load history applied to the aft of the ice sample based on impact test 1. The applied load and the simulated indentation are shown in Figure 13a. The local indentation into the beam flange match the experimental deformation in Figure 9 closely, while the global deflection is somewhat underestimated.

Comparing the applied force vs. indentation, it is also clear that impact tests no. 2-4, in which the ice failed globally at less than 75 kN, caused no significant permanent damage to the beam in the experiments. Further, as the failure mode was local indentation to the beam flange which then caused global deformation of the beam, extending the beam span from 700 mm in test 1 to 900 and 800 mm in tests 2-4 reduced the strength of the beam, thereby giving lower local damage.



a) Applied load and simulated global and local indentations to the beam for test 1.

b) Deformation of beam in numerical simulation at the point of maximum plastic damage. Fringes are in [mm].

Figure 13 Results of numerical evaluation of beam strength.

Figure 13b shows a cross-section of the beam response to the collision load at the point at which the indentation into the beam match the permanent damage as in Figure 9. As the beam wraps around the ice tip it confines the ice locally, thereby increasing its crushing strength even for small levels of indentation.

Amplified force fluctuations were observed in the beam simulations at the simply supported boundary. Thus, the simple numerical simulation supports that the force oscillations with a period of around 1 ms observed in all the impact tests was due to the coupled ice crushing and the beam vibration (both local flange and global beam). After the applied load signal, the beam vibrates freely with a period of 2.35 ms, close to the first natural vibration mode. Further studies are needed to investigate the coupled vibrational response, and refined measurements should be employed in future experiments if the natural frequency of the impacted structure is not increased significantly.

DISCUSSION AND CONCLUSIONS

Experiments on coupled ice-structure interaction in the brittle ice regime were successfully conducted. Permanent damage of both the ice and the steel structure was obtained, and the experimental setup and procedure was found to be suitable for further studies of the coupled ice-structure behaviour. The high sampling rates of both forces and high-speed video proved very useful to be able to observe the ice response. For example, a crack propagating through the specimen took between two to four frames, thereby having a propagation speed between 1500 and 3000 m/s.

Plastic damage to the beam was only observed for impact test 1. This was likely due to a combination of two factors. Firstly, the pre-existing circumferential crack allowed for a larger contact area to be established prior to global failure of the ice. This could also have been achieved with a flat tip of the ice specimen. Secondly, when the beam flange deformed, its confining effect increased the crushing strength of the ice, thereby causing even larger damage to the beam. This highlights that the transition between a near rigid structure and large inelastic deformations (strength design vs. shared energy design) is very narrow, and small changes in the collision scenario may significantly change the outcome in terms of structural deformation, similar to ship-ship collisions in Storheim and Amdahl (2014).

Further investigations of this coupled effect are vital to improve the understanding of ice in a realistic impact scenario, and to establish additional requirements to limit catastrophic damage on vessels with design loads with high probabilities (less than 100 year return period). This can be achieved through a combination of rigid and deformable impacted structures as well as impacts at different velocities but the same kinetic energy. Performing such experiments in the pendulum accelerator is shown to be a viable option.

ACKNOWLEDGEMENTS

This work was supported in parts by the Research Council of Norway through the Centres of Research-based Innovation funding scheme, projects SAMCOT and SIMLab. Trond Auestad and Tore Wisth from SIMLab are acknowledged for the invaluable technical assistance during the experiments.

REFERENCES

- Barrette, P.D. and Jordaan, I.J., 2001. Beam bending and fracture behaviour of iceberg ice. PRED/CHC report 4-78, Ocean Engineering Research Center, Memorial University of Newfoundland.
- Gagnon, R.E. and Gammon, P.H., 1995. Characterization and flexural strength of iceberg and glacier ice. *Journal of Glaciology* 41(137), 103–111.

- Gudimetla, P. S., Colbourne, B., Daley, C., Bruneau, S. E., & Gagnon, R. 2012. Strength and Pressure Profiles from Conical Ice Crushing Experiments. In International Conference and Exhibition on Performance of Ships and Structures in Ice 2012, ICETECH 2012 (pp. 167-174).
- Hänninen, S. 2005. Incidents and accidents in winter navigation in the Baltic Sea, winter 2002-2003. Finnish Maritime Administration.
- Hanssen, A. G., Auestad, T., Tryland, T., & Langseth, M. 2003. The kicking machine: A device for impact testing of structural components. *International Journal of Crashworthiness*, 8(4), 385-392.
- Kim, E., Storheim, M., Amdahl, J., Loset, S., & und Polach, R. V. B. (2013). Drop tests of ice blocks on stiffened panels with different structural flexibility. *Collision and Grounding of Ships and Offshore Structures*, 241.
- Kujala, P., Ehlers, S., 2013, Limit state identification for ice-strengthened hull structures using measured long-term loads, *Proceedings of the 22nd International Conference on Port and Ocean Engineering under Arctic Conditions*, June 9-13, 2013, Espoo, Finland
- Manuel, M., Gudimetla, P.S.R., Daley, C. and Colbourne, B., 2013. Controlled plastic deformation of a grillage using artificial freshwater ice at large scale. *Proceedings of the 22nd International Conference on Port and Ocean Engineering under Arctic Conditions*, Espoo, Finland, Paper POAC13_157.
- Masterson D.M., Frederking, R.M.W., Jordaan, I.J. and Spencer P.A., 1993. Description of multi-year ice indentation tests at Hobson's Choice Ice Island – 1990. *Proceedings of 3rd International Conference on Ocean, Offshore and Arctic Engineering* 4, 145–155.
- Masterson, D. M., & Frederking, R. M. W. 1993. Local contact pressures in ship/ice and structure/ice interactions. *Cold Regions Science and Technology*, 21(2), 169-185.
- Oldford, D. and Sopper, R. and Daley, C. 2014, Impact Ice Loads on Spherical Geometries, ICETECH14-120-RF, *Proceedings of the ICETECH2014 conference*, July 28.-31., Banff, Alberta, Canada
- Riska, K. and Kämäräinen, J., 2011. A Review of Ice Loading and the Evolution of the Finnish-Swedish Ice Class Rules. Draft to the SNAME Annual meeting in 2011, SNAME Transactions, to be published.
- Pettersen, T. (2013). Tanker accident on Northern Sea Route. [online] Barentsobserver. Available at: <http://barentsobserver.com/en/nature/2013/09/tanker-accident-northern-sea-route-09-09> [Accessed 15 Dec. 2014].
- Saeki, H., Hamanaka, K., & Ozaki, A. 1977. Experimental study on ice force on a pile, *Proceedings of the 4th International Conference on Port and Ocean Engineering under Arctic Conditions*, St. Johns , Canada, p 695-706
- Schulson, E. M., & Duval, P. 2009. *Creep and fracture of ice* (p. 432). Cambridge: Cambridge University Press.
- Shazly, M., Prakash, V., & Lerch, B. A. 2009. High strain-rate behavior of ice under uniaxial compression. *International Journal of Solids and Structures*, 46(6), 1499-1515.
- Storheim, M., Amdahl, J. (2014). Design of offshore structures against accidental ship collisions. *Marine Structures*, 37, 135-172.
- Ulan-Kvitberg, C., Kim, H., & Daley, C. 2011. Comparison of pressure-area effects for various ice and steel indenters. In *Proceedings of the 21st International Offshore and Polar Engineering Conference Maui, Hawaii, USA*.
- Varsta, P. and Riska, K., 1982. Measurement of ice pressures and forces on Canmar Kigoriak during repeated trials in 1981. Report LAI-332/82, Technical Research Centre of Finland, Dome Petroleum Limited.